Chemical Engineering Journal 154 (2009) 196–202

Contents lists available at ScienceDirect

Chemical Engineering Journal

journal homepage: www.elsevier.com/locate/cej

Simulation of a membrane reactor for the WGS reaction: Pressure and thermal effects

M. Esperanza Adrover, Eduardo López [1], Daniel O. Borio, Marisa N. Pedernera *

Planta Piloto de Ingeniería Química (Universidad Nacional del Sur, CONICET), Camino La Carrindanga km. 7, 8000 Bahía Blanca, Argentina

ARTICLE INFO

Article history:
Received 27 November 2008
Received in revised form 13 April 2009
Accepted 27 April 2009

Keywords:
Membrane reactor
WGS
Hydrogen production
Pd membrane

ABSTRACT

A simulation study of a membrane reactor for the water-gas shift reaction is presented. A pseudohomogenous 1D mathematical model is considered to describe the performance of the membrane reactor under steady-state operation. The membrane consists on a dense Pd layer (selective to H_2) deposited on a porous ceramic support. The influence of operating pressure and thermal effects on the membrane reactor performance is analyzed and the results are compared with those corresponding to a reactor with no hydrogen permeation.

1. Introduction

Hydrogen production has become an important topic over the past decades, but nowadays it is of greater interest because of fuel cell-technology developments. This situation has intensified the research tending both to improve the existing technologies and to develop new processes to generate and purify H_2.

Reforming or partial oxidation of hydrocarbons or alcohols have been reported as the main processes to obtain the required hydrogen. In most cases, the CO content evolving from the production reactor has to be reduced to avoid the poisoning of the fuel cell anode catalyst. The water-gas shift reaction (WGS, see Eq. (1)) is selected to accomplish this objective with the additional effect of increasing the H_2 production:

$$CO + H_2O \leftrightarrow CO_2 + H_2 \qquad \Delta H^{\circ}_{298\ K} = -41.09\ \text{kJ/mol} \tag{1}$$

The WGS reaction is moderately exothermic and strongly controlled by thermodynamic equilibrium. The equilibrium conversion is favored under low temperatures and is independent of pressure. In fuel cell applications, equilibrium limitations determine the WGS reactor volume as the largest of the generation-purification system [1].

An attractive alternative in order to increase CO conversion is the use of a hydrogen-selective membrane in the WGS reactor. Membrane reactors (MR) have attracted considerable interest since they combine the chemical reaction and the separation in a single unit [2]. The selective permeation through the membrane of some reaction products (e.g., H_2) shifts the equilibrium towards products and consequently the CO conversion increases. Alternatively, the amount of catalyst for a desired conversion level can be reduced when compared with a conventional fixed-bed reactor. The H_2 removal can be performed by using selective dense membranes of Pd and its alloys. In order to decrease the cost and increase the permeation fluxes, composite membranes have become an interesting alternative. These membranes consist on a selective metallic layer (Pd) deposited on a highly porous substrate with low flow rate resistance [3–5].

Many studies have been reported concerning the simulation of water-gas shift membrane reactors (WGS-MR) [4,6]. However, in most cases the thermal effects are neglected and isothermal operation is considered. This assumption is acceptable in low-scale (laboratory) reactors due to the high transfer area/reaction-volume ratios. Nevertheless, when several membrane tubes are installed in parallel inside a shell through which the sweep gas flows, the hypothesis of isothermal operation may no longer be valid. Under these circumstances, thermal effects should be considered [7–9]. In a previous work [10], a theoretical study addressing the influence of thermal effects on a WGS-MR performance and stability was presented, for different configurations of the sweep gas flow on the reactor shell (co- and counter-current). In this way, the sweep gas not only increases the driving force for the hydrogen permeation but also acts as a coolant for the exothermic WGS reaction. However, if the membrane reactor operates with high sweep gas flow rates, the separation step (H_2/sweep gas mixture) after the WGS reactor could limit the use of these reactors.

* Corresponding author. Fax: +54 291 4881600.
E-mail address: mpedernera@plapiqui.edu.ar (M.N. Pedernera).
[1] Currently at Institut de Tecniques Energetiques, Universitat Politecnica de Catalunya, Av. Diagonal 647, ed. Etseib, 08028 Barcelona, Spain.

1385-8947/$ – see front matter © 2009 Elsevier B.V. All rights reserved.
doi:10.1016/j.cej.2009.04.057

An alternative to eliminate the sweep gas could be to increase the feed pressure. As the permeation flux in Pd membranes is normally given by the difference of the square roots of H_2 partial pressures on both sides of the membrane, higher pressures on the reaction side lead to an increase of the permeation driving force.

Brunetti et al. [11] reported the positive effect of higher feed pressures on the CO conversion in a lab-scale MR, by means of a non-isothermal mathematical model. Although the reaction is exothermic, an external oven is required in order to avoid the extinction of the reaction in the selected laboratory reactor (high heat transfer area). However, when the design is scaled-up, the reactor should be operated adiabatically or with an external coolant.

The aim of the present contribution is to analyze the effect of the pressure on the performance of a MR for the WGS upstream of a 10 kWth PEM fuel cell, with special focus on the thermal effects associated with this operation. Both convective (with its associated U) and diffusive (due to hydrogen permeation) heat transfer mechanisms are considered to quantify the energy transport through the membrane. The complete unit is considered globally adiabatic (with respect to the environment). The results are compared with those of a conventional fixed-bed reactor (CR). A pseudohomogeneous mathematical model has been selected to represent the operation of both reactor designs (MR and CR).

2. Mathematical model

The selected design for the MR considers several membrane tubes installed in parallel within a shell (Fig. 1). The catalyst is packed in the shell side and a hydrogen stream is collected in the inner side of the membrane tubes. As no sweep gas is considered, pure H_2 is produced on the permeate side.

In order to describe the steady-state operation of the membrane reactor a 1D mathematical model is considered, under the following hypothesis:

(a) Axial dispersion terms of mass and energy are neglected.
(b) Composition and thermal gradients in the radial coordinate are neglected.
(c) Isobaric conditions.
(d) Ideal membrane only permeable to hydrogen (infinity selectivity).
(e) Co-current flow between the feed and permeate streams is assumed.
(f) The reactor is globally adiabatic (with respect to the environment, no external coolant).

The Langmuir–Hinshelwood kinetic model proposed by Podolski and Kim [12] is selected to evaluate the reaction rate.

Under the stated hypothesis, the reaction model is:

Shell side (catalyst bed):

Mass balances

$$\frac{dF_{CO}}{dz} = A_T\, r_{CO}\, \rho_B \tag{2}$$

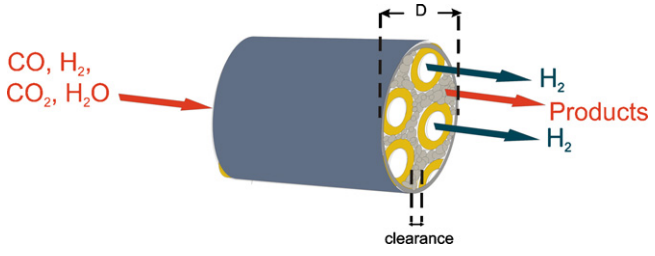

Fig. 1. Scheme of the multitubular membrane reactor.

$$\frac{dF_{H_2}}{dz} = A_T(-r_{CO})\rho_B - \pi n d_{te} J_{H_2} \tag{3}$$

Molar flow rates for other species present in the reaction medium (CO_2, CH_4 and H_2O) are calculated from overall molar balances.

Energy balance

$$\frac{dT}{dz} = \frac{A_T \rho_B(-r_{CO})(-\Delta H_r) - \pi\, n\, d_{ti} U(T - T_P)}{\sum_{j=1}^{N} F_j C_{pj}} \tag{4}$$

Tube side (permeate stream):

Mass balances

$$\frac{dF_{H_2,P}}{dz} = \pi d_{te} J_{H_2} \tag{5}$$

Energy balance

$$\frac{dT_P}{dz} = \frac{\pi d_{te}}{F_{H_2,P} C_{pH_2}} \left[J_{H_2} C_{pH_2} + U \frac{d_{ti}}{d_{te}} \right] (T - T_P) \tag{6}$$

Boundary conditions:

$$\text{at } z = 0 \begin{cases} F_j = F_{jo} \quad \text{for} \quad j = 1, 2 \ldots, N \\ T = T_o; T_P = T_o \\ F_{H_2,P} = 0; \end{cases} \tag{7}$$

The hydrogen permeation flux through the membrane is calculated using Sievert's Law [13]:

$$J_{H_2} = \frac{Q_0 e^{(-E/RT)}}{\delta} [\sqrt{p_{H_2}} - \sqrt{p_{H_2,P}}] \tag{8}$$

where δ is the membrane thickness and p_{H_2} and $p_{H_2,P}$ are the hydrogen partial pressures on the reaction and permeation sides, respectively.

The overall heat transfer coefficient (U) is evaluated using the following equation:

$$U = \frac{1}{(d_{ti}/d_{tm})(1/\alpha_r) + r_{ti}(\ln(d_{te}/d_{ti})/k_{Al_2O_3}) + r_{ti}(\ln(d_{tm}/d_{te})/k_{Pd}) + 1/\alpha_P} \tag{9}$$

The overall convective heat transfer coefficient in the retentate side (α_r) is estimated following the guidelines reported by Dixon [15]:

$$\frac{1}{\alpha_r} = \frac{1}{\alpha_w} + \frac{r_{eq}}{3k_{er}} \frac{Bi + 3}{Bi + 4} \tag{10}$$

where, the wall heat transfer coefficient (α_w) and the effective radial heat conductivity (k_{er}) are calculated using the correlations proposed by Dixon and Cresswell [14].

These correlations have been developed for a tubular configuration. However, they could be used for annular configuration as proposed by De Falco et al. [16] by means of an equivalent radius (r_{eq}). The heat transfer coefficient corresponding to the permeate side (α_P) is evaluated for laminar, fully developed flow from Incropera and DeWitt [17]. The heat conductivity of the support ($k_{Al_2O_3}$) and the Pd membrane (k_{Pd}) are obtained from Hussain et al. [18] and Incropera and DeWitt [17], respectively.

The CR is modelled by considering that the hydrogen flow through the membrane is equal to zero ($J_{H_2} = 0$).

The design parameters and the operating conditions used in the simulations are presented in Table 1.

3. Results and discussion

3.1. Reactor design

Fig. 2 shows the effect of adding membrane tubes on the dimensionless permeance of H_2 for different retentate pressures. The

Table 1
Geometric parameters and operating conditions used to simulate the MR and CR.

d_{ti}	8 mm[a]	F_{T0}	345 mol/h (ca. 10 kW[a])
d_{te}	13.4 mm[a]	CO, %	7.97[b]
d_P	1 mm	CO_2, %	10.99[b]
$V_{cat,T}$	2260 cm[a]	H_2, %	43.48[b]
δ	60 μm[a]	H_2O, %	31.88[b]
P_p	1 atm[a]	CH_4, %	5.6 K[b]

[a] Criscuoli et al. [4].
[b] Francesconi et al. [1].

dimensionless permeation flow is defined as the quotient between the hydrogen flow permeated through the membrane ($F_{H_2,P}$) and the maximum amount of hydrogen that could be produced, i.e. when all CO reacts, given by:

$$F^{max}_{H_2,P} = F_{H_2,o} + F_{CO,o} \quad (11)$$

All the curves presented in Fig. 2 are obtained by keeping constant both the reactor length/shell-diameter ratio ($L/D = 2$) and the catalyst volume ($V_{cat} = 2260\,cm^3$). For a given pressure (P), D increases with the tube number (n) to maintain the same amount of catalyst and so does L to keep a constant ratio L/D, while the distance between tubes diminishes. In this work, a minimum clearance between tubes equivalent to four times the particle diameter is adopted to maintain an appropriate flow distribution. From Fig. 2, it is clear that the permeation flow increases with the number of membrane tubes (n), i.e. with the permeation area. At each operating pressure, the horizontal dotted line corresponds to the dimensionless hydrogen permeation flow for the maximum allowed area, i.e., the configuration with the minimum separation between tubes.

For all the possible configurations of the MR, the H_2 permeation flow increases with the retentate pressure as a consequence of the increase of the driving force for the permeation.

In order to study the operation of different MR configurations, two conditions in Fig. 2 (cases A and B) leading to the same H_2 permeation are selected. Point A corresponds to a MR with low permeation area ($n = 20$) operating at high pressure (30 atm); conversely, point B represents an operation at a lower pressure (7 atm) but with the highest allowed permeation area (i.e., $n = 63$).

Axial profiles of CO conversion, temperature and reaction rate are presented in Fig. 3 for the cases A and B of Fig. 2.

In the first section of the reactor, the higher retentate pressure of case A leads to a higher reaction rate and a higher H_2 permeation flux (J_{H_2}) due to the increase of the driving force. As a result, a significant difference between the temperatures of the retentate and permeate streams is observed.

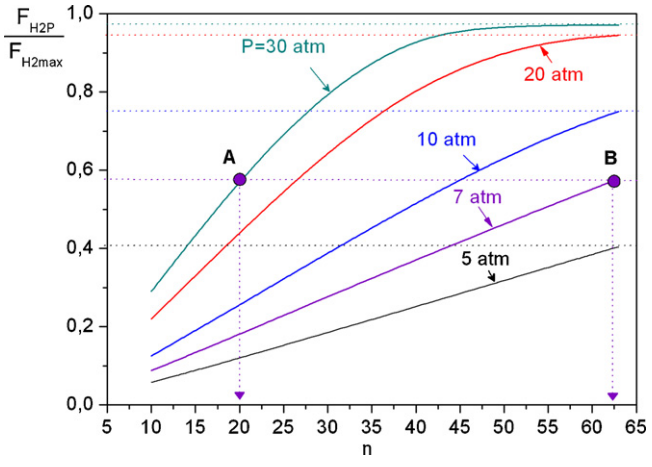

Fig. 2. Dimensionless H_2 permeation flow as a function of the number of tubes and the operating pressure (shell side).

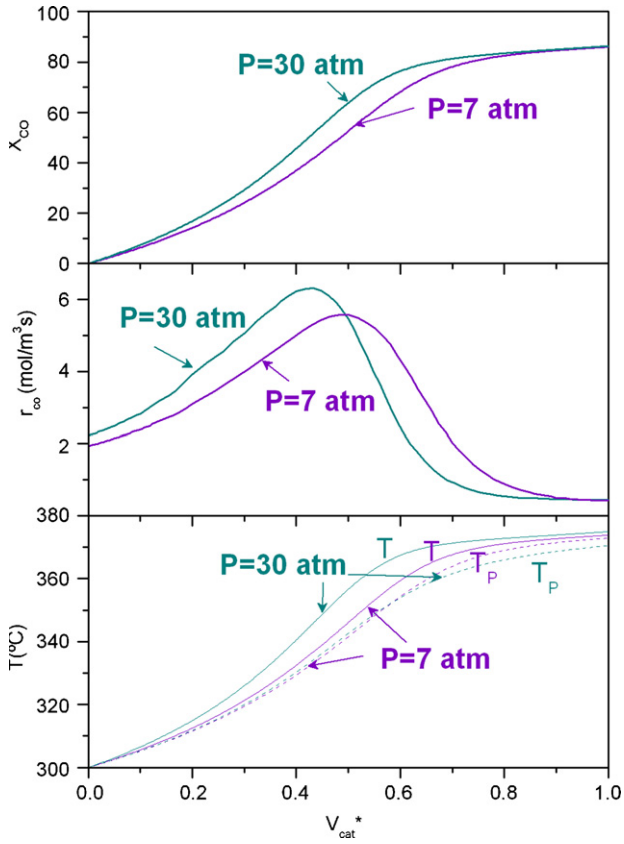

Fig. 3. X_{CO}, reaction rate and temperature profiles for points A and B of Fig. 2 (full lines: shell side, dotted lines: tube side).

In the back axial section of the reactor, the H_2 permeance of case B enhances and so does the reaction rate due to the higher permeation area. In this case, the temperature difference between the streams is smaller.

Finally, even though the operating conditions of the studied cases are very different, both outlet CO conversions are similar since the total amount of permeating H_2 is approximately the same (see Fig. 2).

These results suggest a trade off between capital costs associated to permeation areas and operating costs related to operating conditions (higher pressures). In the following sections of the present contribution, a MR design corresponding to $n = 63$ is selected.

3.2. Pressure and thermal effects

In this section, the thermal effects associated to the MR operation at different pressures are studied. Initially, the simulation of the MR is performed neglecting the convective heat transfer phenomenon ($U = 0$), i.e. the energy transfer between the process and permeate streams is only due to the permeation flux.

In Fig. 4, conversion profiles along the reactor for different inlet feed pressures are presented. For comparison purposes, the profile corresponding to $P = 5$ atm for the conventional reactor ($J_{H_2} = 0$) is also shown. As it is shown in Fig. 4, the operating pressure has a strong influence on the performance of the MR. In fact, higher pressures lead to an increase of the CO conversion due to higher H_2 permeation flows, e.g. when pressure increases from 5 to 10 atm, X_{co} raises 10%, and 18% when it increases to 20 atm. These higher productions are associated with higher thermal effects due to the exothermicity of the reaction, as shown in Fig. 5 (same operating conditions of Fig. 4).

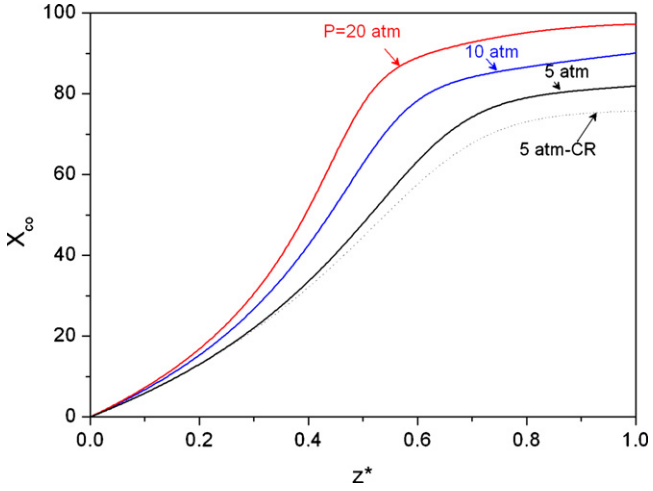

Fig. 4. CO conversion axial profiles for different pressures. $U=0$ and $T_o=300\,^{\circ}C$.

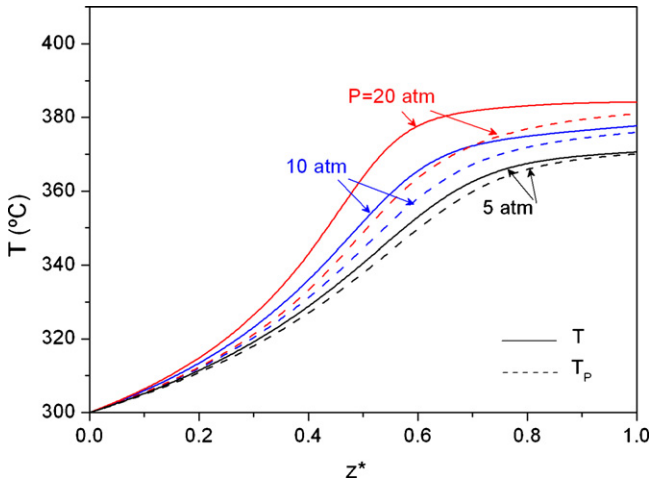

Fig. 6. Axial temperature profiles of retentate and permeate sides for different pressures (U calculated by Eq. (9)).

The increment of the operating pressure affects the retentate temperature in a higher extent, enlarging the temperature differences between the streams on both sides of the membrane. It is worth reminding that the heat transfer from the reaction side to the permeate side is only a consequence of the H_2 permeation flux, as the convective heat transfer is neglected ($U=0$) (see Eqs. (4) and (6)).

When the heat transfer coefficient (U) is evaluated using correlations as described in Eq. (9) ($U\cong 15$–$25\,W/m^2K$), the CO conversion for a given pressure does not experience any significant variation when compared to $U=0$, as it will be seen in temperature-conversion trajectories afterwards. Therefore, the total heat generated by the reaction is approximately the same under both heat transfer conditions. However, the axial temperature profiles show a noticeable change, as shown in Fig. 6 for different retentate pressures. Due to an improvement of the heat exchange between the retentate and permeate sides, the difference $(T-T_P)$ diminishes when compared with the case $U=0$ (see Fig. 5).

At this point, it is important to compare the results of the present work with those presented by Brunetti et al. [11]. These authors simulated a lab-scale reactor which is installed inside a furnace in order to prevent the reaction extinction due to heat losses to the environment. In the present paper, a bigger reactor scale is selected, leading to a diminution of the shell-environment heat transfer area and, therefore, allowing the supposition of adequate shell isolation to permit adiabatic operation. As a result, the temperature rises along the reactor length reported by Brunetti et al. [11] are considerably higher than those calculated in the present article.

If the heat transfer coefficient continues increasing, even tending to infinity, the temperature profiles of retentate and permeate sides should almost overlap. In fact, as shown in Fig. 7, simulations considering very high values for U ($U\to\infty$) show minimum temperature differences for all the operating pressures.

Fig. 8 shows the temperature (process gas)-conversion trajectories for different pressures, when $U\to\infty$. The result for the conventional reactor (CR, $U=0$) is also included. As shown, all the trajectories overlap the adiabatic line of the CR and finish at increasing conversions as the pressure increases. Due to the simulated infinite rate for the convective heat exchange ($U\to\infty$), the heat generated by the reaction at all axial positions is immediately distributed between the retentate and permeate streams leading to equal temperatures. As the operation of the MR as a whole is assumed globally adiabatic (i.e., no external coolant and adiabatic shell to the environment are considered), the temperature of both streams follows the adiabatic operation line.

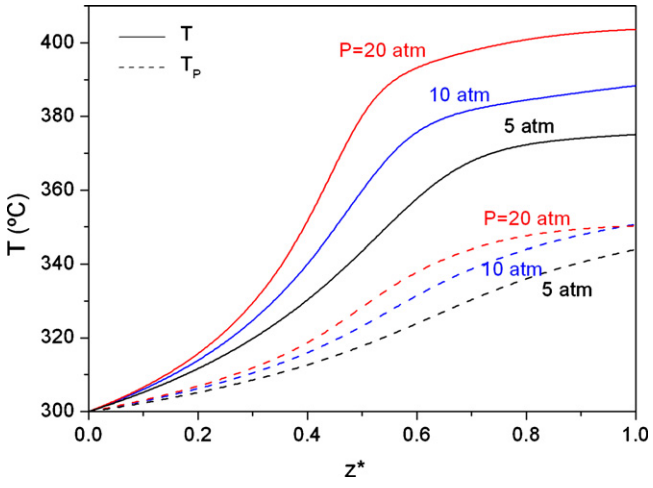

Fig. 5. Axial temperature profiles of retentate and permeate sides for different pressures on the shell side. $U=0$ and $T_o=300\,^{\circ}C$.

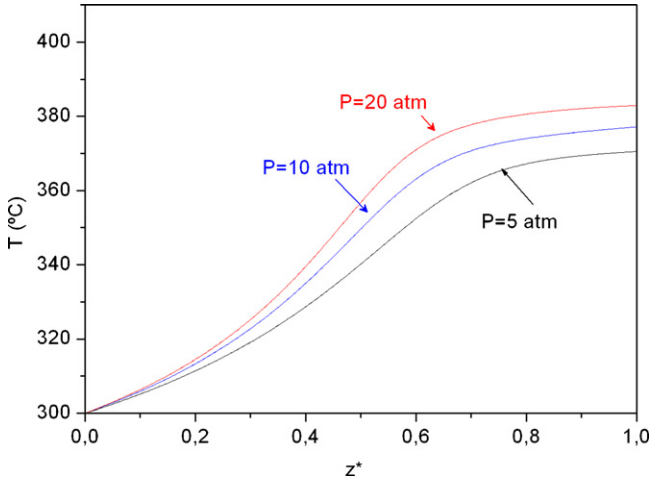

Fig. 7. Axial temperature profiles of retentate and permeate sides for different pressures ($U\to\infty$).

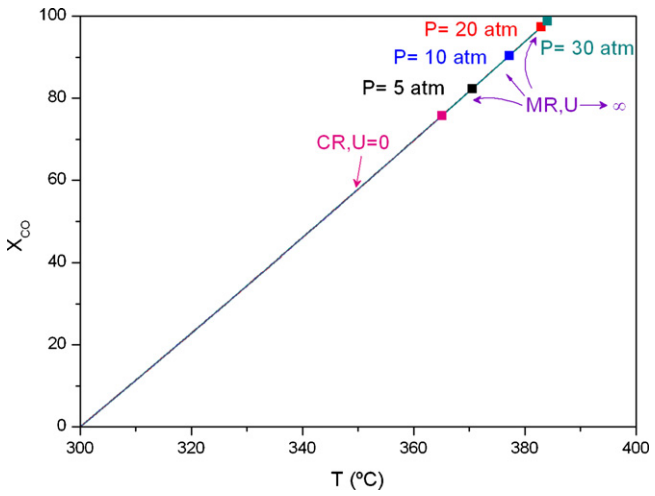

Fig. 8. Temperature–X_{CO} trajectories for different pressures ($U \to \infty$). T_o = 300 °C. Full squares represent temperature and conversion at $z = L$.

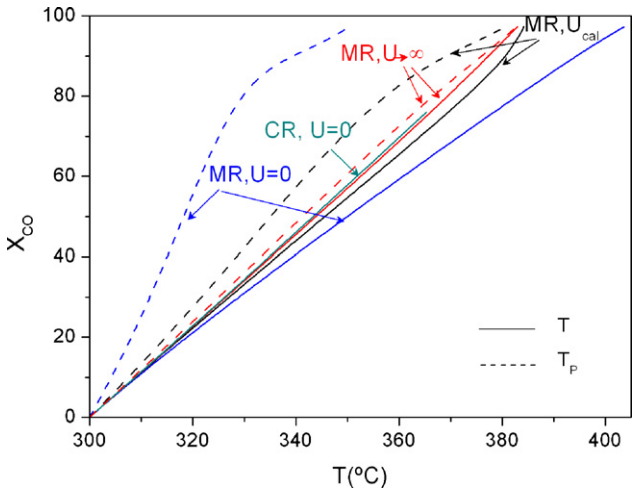

Fig. 10. Temperature–X_{CO} trajectories for different values of U; P = 20 atm. Same operating conditions as Fig. 9.

Axial temperature profiles for the studied cases regarding the simulation of the convective heat transfer ($U = 0$, U calculated and $U \to \infty$) at P = 20 atm are presented in Fig. 9. The corresponding T–X_{CO} and T_P–X_{CO} trajectories are shown in Fig. 10. Once more, the outlet CO conversion is similar for all the studied cases but the axial temperatures on both sides of the membrane vary considerably due to the different forms in which the streams exchange heat.

As illustrated in Fig. 9, T and T_P profiles approach each other as the heat transfer between the streams is improved, i.e. when the heat transfer coefficient is increased. Fig. 10 sums up the aforementioned remarks. It is worth remarking that the cases corresponding to $U = 0$ and $U \to \infty$ are theoretical operating conditions for a specified pressure and only the simulations with U calculated from correlations represent the operation of a real MR.

In Fig. 10, the process gas trajectory for the MR when considering a negligible heat transfer contribution ($U = 0$) is described by the following equation:

$$\frac{dx_{CO}}{dT} = \frac{1}{\Delta T_{ad}} \left(\frac{F_T}{F_{To}} \right) \tag{12}$$

which results from combining mass and energy balances of the reaction side (Eqs. (2) and (6)). As seen, the T–X_{CO} curve shifts from the typical straight line of the CR with slope $1/\Delta T_{ad}$. The temperature increase due to higher conversions and the decrease in the molar flow rate along the axial coordinate produce an additional temperature increment in the MR. In other words, the term F_T/F_{To} of Eq. (12) diminishes gradually in the MR as the reaction takes place and hydrogen is permeated through the membrane, while in the CR ($J_{H_2} = 0$) this term is unitary. Consequently, as the H_2 permeation increases, the trajectories of the MR shift from the straight line of the CR in a greater extent. The case with $U = 0$ shows the maximum possible deviation from the adiabatic CR line. As U increases, process gas and permeated-gas temperatures approach each other, reaching the opposite limit in the already described situation with $U \to \infty$, when both (T and T_P) trajectories overlap the adiabatic CR line. In all situations, temperatures must close the overall heat balance of an adiabatic membrane reactor.

When all the hydrogen in the process gas mixture (i.e., generated H_2 by reaction and H_2 originally in the feed) permeates through the membrane, the reaction may be considered irreversible and the minimum ratio between flow rates (F_T/F_{To}) can be expressed as

$$\frac{F_T}{F_{To}} = 1 - (y_{H_2,o} + y_{CO,o}) \tag{13}$$

The maximum temperature increment that could be reached in an adiabatic membrane reactor can be calculated relating Eqs. (12) and

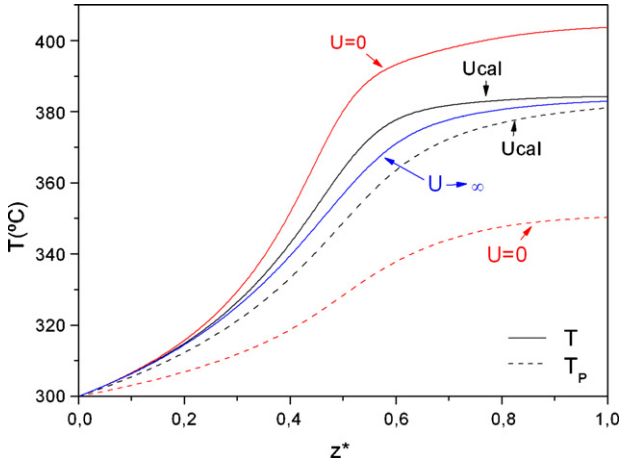

Fig. 9. Temperature axial profiles of retentate and permeate sides for different U for P = 20 atm. T_o = 300 °C.

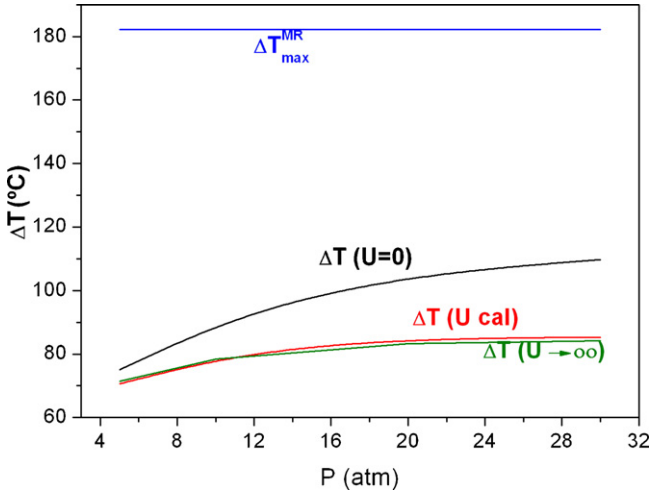

Fig. 11. Inlet–outlet temperature increment in a MR as a function of the operating pressure, for different values of U.

(13):

$$\Delta T_{\max}^{MR} = \Delta T_{ad}\left(\frac{F_{To}}{F_T}\right) = \frac{\Delta T_{ad}}{(1 - y_{H_2,o} - y_{CO,o})} \quad (14)$$

Fig. 11 shows the differences between the inlet and outlet temperature in the MR as a function of the retentate pressure for $U = 0$, U calculated and $U \to \infty$. The maximum temperature increment achievable in an adiabatic MR ($\Delta T_{\max}^{MR}$) is also included. As it can be observed, very high pressures would be required in order to reach this limit situation.

4. Conclusions

The present contribution deals with the theoretical analysis of a membrane reactor operation for the water-gas shift reaction for fuel cell applications. The influence of operating pressure and thermal gradients on the reactor performance is mainly addressed. A design considering a multi-tubular membrane reactor with the catalyst in the shell and co-current flow of the permeated hydrogen inside the tubes is selected. No sweep gas is considered to obtain pure hydrogen and eliminate any downstream purification unit.

Different combinations of operating conditions and reactor designs (length and number of tubes) lead to the same reactor performance. The final design must, therefore, rely on additional considerations as a cost evaluation, studies of integration of the unit in the overall production device, etc.

The MR leads to higher CO conversions than the CR due to the shift of equilibrium caused by hydrogen permeation. Although, the process gas in the MR experiences a higher temperature rise than that of the conventional fixed-bed reactor (due to higher conversions and diminution of the flow rate), this increment is minimized in the selected design by using a high heat transfer area. An increase in the process gas pressure leads to an important improvement in CO conversion. This also increases the temperature rise inside the reactor (for all cases analyzed regarding U values). At a fixed pressure, the partition of the generated heat between the process and the permeate streams leads to: $(T–T_o)_{(U\to\infty)} < (T–T_o)_{(Ucalc)} < (T–T_o)_{(U=0)}$.

For high values of (UA), the membrane reactor (MR) operates "tracking" the trajectory of the adiabatic conventional reactor (CR, for $U = 0$), i.e.: $T - T_o \approx T_P - T_o = \Delta T_{ad} X_{CO}^{MR}$. Nevertheless, the conversion in the MR (X_{CO}^{MR}) is higher than the corresponding to the CR and consequently the MR shows a higher temperature rise.

As the pressure on the retentate side increases and the heat transfer area diminishes, the temperature rise in the catalyst bed ($T–T_o$) may be considerably higher than the value given by aforementioned equation, i.e.: $(T–T_o)^{MR} \gg \Delta T_{ad} X_{CO}$.

Nomenclature

A_T	cross-sectional area of shell (m^2)
Bi	Biot number
C_p	heat capacity (kJ/(mol K))
d	diameter of tube (m)
D	shell-diameter (m)
E	activation energy (J/mol)
F	molar flow rate (mol/s)
J_{H_2}	permeation flow of H_2 (mol/(s m^2))
k	heat conductivity (W/(m K))
L	tube length (m)
N	total number of components (reaction side)
n	tube number
p_{H_2}	partial pressure of H_2 (atm)
Q_0	pre-exponential factor in the Arrhenius relationship (mol/(s m $atm^{0.5}$))
r	radius (m)
r_{CO}	reaction rate ($mol_{CO}/(kg_{cat}$ s))
P	pressure (atm)
T	temperature (K)
U	overall heat transfer coefficient (W/(m^2 K))
V	catalyst volume (cm^3)
W	catalyst mass (g)
y	molar fraction of component
x	conversion
z	axial coordinate (m)

Greek letters

α	heat transfer coefficient (W/(m^2 K))
δ	thickness of the Pd layer (m)
ΔH_r	heat of reaction (kJ/mol)
$\Delta T_{ad} = \frac{(-\Delta H_r) y_{CO,o}}{\bar{C}_p}$	adiabatic temperature rise (K)
ρ_B	fixed-bed density (kg_{cat}/m^3)

Superscript

*	dimensionless

Subscripts

cat	catalyst
j	component *j*
MR	membrane
P	permeate side or particle
r	retentate side or radial
T	total
te	external tube
th	thermal
ti	internal tube
tm	membrane tube (external + Pd layer)
eq	equivalent
er	effective radial
o	at the axial coordinate $z = 0$
L	at the axial coordinate $z = L$
w	wall
ad	adiabatic

Acknowledgements

The authors acknowledge Universidad Nacional del Sur (UNS), Consejo Nacional de Investigaciones Científicas y Tecnológicas (CONICET) and Agencia Nacional de Promoción de Ciencia y Tecnología (ANPCyT) for the financial support.

References

[1] J.A. Francesconi, M.C. Mussati, P. Aguirre, Analysis of design variables for water-gas-shift reactors by model-based optimization, Journal of Power Sources 173 (2007) 467–477.
[2] J. Coronas, J. Santamaría, Catalytic reactors based on porous ceramic membranes, Catalysis Today 51 (1999) 377–389.
[3] S. Tosti, L. Bettinali, V. Violante, Rolled thin Pd and Pd–Ag membranes for hydrogen separation and production, International Journal of Hydrogen Energy 25 (2000) 319–325.
[4] A. Criscuoli, A. Basile, E. Drioli, An analysis of the performance of membrane reactors for the water-gas shift reaction using gas feed mixtures, Catalysis Today 56 (2000) 53–64.
[5] X. Li, T.M. Liu, Y.Q. Fan, N.P. Xu, Preparation of composite palladium-silver alloy membranes by photocatalytic deposition, Thin Solid Films 516 (2008) 7282–7285.
[6] A. Basile, L. Paturzo, F. Gallucci, Co- and counter-current modes for water gas shift membrane reactor, Catalysis Today 82 (2000) 275–281.
[7] M. De Falco, P. Nardella, L. Marrelli, L. Di Paola, A. Basile, F. Gallucci, The effect of heat-flux profile and of other geometric and operating variables in designing

industrial membrane methane steam reformers, Chemical Engineering Journal 138 (2008) 442–451.
[8] M. Koukou, G. Chaloulou, N. Papayannakos, N. Markatos, Mathematical modeling of the performance of non-isothermal membrane reactors, International Journal of Heat and Mass Transfer 40 (1997) 2407–2417.
[9] N. Itoh, T. Wu, An adiabatic type of palladium membrane reactor for coupling endothermic and exothermic reactions, Journal of Membrane Science 124 (1997) 213–222.
[10] M.E. Adrover, E. López, D. Borio, M. Pedernera, Heat effects in a membrane reactor for the water gas shift reaction Studies on Surface Science and Catalysis, 167, Elsevier, Amsterdam, 2007, pp. 183–188.
[11] A. Brunetti, A. Caravella, G. Barbieri, E. Drioli, Simulation study of water gas shift reaction in a membrane reactor, Journal of Membrane Science 306 (2007) 329–340.
[12] W.F. Podolski, Y.G. Kim, Modeling the water-gas shift reaction, Industrial and Engineering Chemistry 13 (4) (1974) 415–421.
[13] G. Barbieri, A. Brunetti, T. Granato, P. Bernardo, E. Drioli, Engineering evaluations of a catalytic membrane reactor for the water gas shift reaction, Industrial and Engineering Chemistry Research 44 (2005) 7676–7683.
[14] A.G. Dixon, D.L. Cresswell, Theoretical prediction of effective heat transfer parameters in packed beds, AIChE Journal 25 (4) (1979) 663–676.
[15] A.G. Dixon, An improved equation for the overall heat transfer coefficient in packed beds, Chemical Engineering and Processing 35 (1996) 323–331.
[16] M. De Falco, L. Di Paola, L. Marrelli, Heat transfer and hydrogen permeability in modelling industrial membrane reactors for methane steam reforming, International Journal of Hydrogen Energy 32 (14) (2007) 2902–2913.
[17] F.P. Incropera, D.P. DeWitt, Fundamentos de transferencia de calor y masa, Prentice Hall Inc., México, 1999.
[18] A. Hussain, A. Seidel-Morgenstern, E. Tsotsas, Heat and mass transfer in tubular ceramic membranes for membrane reactors, International Journal of Heat and Mass Transfer 49 (2006) 2239–2253.